12 Degrees of Freedom Muscle Force Driven Fibril-Reinforced Poroviscoelastic Finite Element Model of the Knee Joint

A. Esrafilian, L. Stenroth, M. E. Mononen, P. Tanska, S. Van Rossom, D. G. Lloyd, I. Jonkers, and R. K. Korhonen

***Abstract*— Accurate knowledge of the joint kinematics, kinetics, and soft tissue mechanical responses is essential in the evaluation of musculoskeletal (MS) disorders. Since in vivo measurement of these quantities requires invasive methods, musculoskeletal finite element (MSFE) models are widely used for simulations. There are, however, limitations in the current approaches. Sequentially linked MSFE models benefit from complex MS and FE models; however, MS model's outputs are independent of the FE model calculations. On the other hand, due to the computational burden, embedded (concurrent) MSFE models are limited to simple material models and cannot estimate detailed responses of the soft tissue. Thus, first we developed a MSFE model of the knee with a subject-specific MS model utilizing an embedded 12 degrees of freedom (DoFs) knee joint with elastic cartilages in which included both secondary kinematic and soft tissue deformations in the muscle force estimation (inverse dynamics). Then, a muscle-force-driven FE model with fibril-reinforced poroviscoelastic cartilages and fibril-reinforced poroelastic menisci was used in series to calculate detailed tissue mechanical responses (forward dynamics). Second, to demonstrate that our workflow improves the simulation results, outputs were compared to results from the same FE models which were driven by conventional MS models with a 1 DoF knee, with and without electromyography (EMG) assistance. The FE model driven by both the embedded and the EMG-assisted MS models estimated similar results and consistent with experiments from literature, compared to the results estimated by the FE model driven by the MS model with 1 DoF knee without EMG assistance.**

Manuscript received March 9, 2020; revised September 16, 2020; accepted November 6, 2020. Date of publication November 11, 2020; date of current version February 26, 2021. This work was supported in part by the European Union's Horizon 2020 research and innovation programme under the Marie Sklodowska-Curie Grant 713645, in part by the Academy of Finland under Grant 286526, Grant 324529, Grant 324994, and Grant 328920, in part by the Sigrid Juselius Foundation, and in part by the Päivikki and Sakari Sohlberg Foundation. *(Corresponding author: A. Esrafilian.)*

A. Esrafilian, L. Stenroth, M. E. Mononen, P. Tanska, and R. K. Korhonen are with the Department of Applied Physics, University of Eastern Finland, 70210 Kuopio, Finland (e-mail: amir.esrafilian@uef.fi).

S. Van Rossom and I. Jonkers are with the Department of Movement Sciences, Human Movement Biomechanics Research Group, KU-Leuven, 3001 Leuven, Belgium.

D. G. Lloyd is with the Griffith Centre for Biomedical and Rehabilitation Engineering (GCORE), Menzies Health Institute Queensland and the Advanced Design and Prototyping Technologies Institute, Griffith University, Gold Coast, QLD 4222, Australia, and also with the School of Allied Health Sciences, Griffith University, Gold Coast, QLD 4222, Australia.

This article has supplementary downloadable material available at https://doi.org/10.1109/TNSRE.2020.3037411, provided by the authors.

Digital Object Identifier 10.1109/TNSRE.2020.3037411

***Index Terms*— Multiscale modeling, Musculoskeletal modeling, finite element analysis, knee joint, electromyography (EMG), elastic foundation.**

I. Introduction

BODY kinematics and kinetics, muscle and ligament forces, and consequently soft tissue mechanical responses to the joint contact forces (JCFs) play crucial roles in the onset and progression of musculoskeletal (MS) disorders [1]–[5]. Since direct measurement of the JCFs, as well as the soft tissue mechanical responses, require invasive methods [6]–[8], numerical methods such as MS and finite element (FE) modeling are widely utilized. The MS modeling is used to estimate joint kinematics, muscle forces, and joint kinetics consistent with the experimental motion and external forces due to the interaction of the body with the environment [9]–[12]. On the other hand, the FE modeling can provide detailed insights into the joint tissue responses with complex material definitions and predefined boundary conditions [13].

The state-of-the-art studies have introduced multiscale musculoskeletal finite element (MSFE) approaches using either sequential or embedded (concurrent) MS and FE models. In a sequential approach, a MS model is used to estimate joint kinematics, external joint moments, muscle forces, and consequently the JCF to drive a FE model [2], [14], [15]. Since the MS and the FE models are in series, highly complicated material models such as fibril-reinforced hyperelastic [14] or fibril-reinforced poroviscoelastic (FRPVE) [2], [15] materials can be employed to model the joint's soft tissues including cartilage and menisci. Nonetheless, a major limitation of the sequential approach is that the MS estimations are independent of the FE model calculations i.e. soft tissue deformations [2], [14], [15]. In other words, the soft tissue deformation estimated by the FE model could alter the secondary kinematics. Consequently, the altered secondary kinematics could substantially affect the muscle parameters (such as moment arm and muscle-tendon length), the JCF, and as a result, tissue mechanical responses [16]–[18].

In contrast to the sequential approach, an embedded workflow utilizes a MS model with an embedded elastic foundation or a FE model. Then, an iterative algorithm with a feedback loop from the elastic foundation model (or a FE model)

informs the MS model of the soft tissue deformations and/or secondary kinematics to re-estimate muscle forces accordingly. Although the embedded (concurrent) method considers soft tissue deformations in the muscle force estimation, the computational burden limits the approach to optimization-based muscle force estimation and simple material models such as rigid bodies [18], [19] or elastic foundation models [20]. Simpler material models may be used to estimate equivalent tissue responses compared to a poro(visco)elastic model during a dynamic, short-term loading [21] as the fluid does not flow out from the tissue. However, in the case of long-term loading, the fluid will flow out of the tissue leads to a time-dependent mechanical relaxation response that can be captured with the poro(visco)elastic material model. Besides, during dynamic loading, the fluid pressurization inside the tissue carries ∼75-90% of the total applied load [22], [23]. This fluid pressurization is significantly affected in joint disorders such as early knee OA and could not be considered in non-porous material models [24], [25]. Moreover, previous studies have shown that non-fibrillar material models cannot accurately calculate the stresses within a fibrillar tissue such as cartilage and a fibril-reinforced material model should be utilized for accurate simulations [26], [27]. All of the aforementioned quantities are known to play a vital role in governing degradative and adaptive responses of soft tissues [5], [24], which emphasize the use of a fibril-reinforced poroviscoelastic (FRPVE) material model. But, none of the studies using the embedded approach [18], [20] have included menisci despite their crucial role in load distribution and stress concentration within cartilage [28], [29]. To the best of our knowledge, none of the previous studies have integrated a FRPVE FE model with a MS model with an embedded 12 DoFs knee joint into a single modeling framework, which could include knee secondary kinematics, soft tissue deformations, and joint contact pressures in the muscle force estimations and then could estimate detailed mechanical responses of the knee cartilage.

Regardless of the aforementioned modeling approaches and their limitations, the minimal number of DoFs for a representative model of the knee joint and the necessity of a subject-specific geometry in the MS model are still unclear. Marra *et al.* (2015) compared a 1 DoF knee joint model with a 12 DoFs knee joint model and concluded that the increase of the DoFs in the knee joint model might result in more accurate secondary kinematics, but less accurate JCF predictions [30]. Nonetheless, several recent studies suggest that a 12 DoFs knee joint MS model with deformable soft tissues has a substantial effect on muscle parameters (such as moment arm and muscle-tendon length), the JCF, and consequently, tissue responses [16]–[18]. In contrast, some studies have shown that a subject-specific electromyography-informed (EMG-informed) MS model [31] or an EMG-assisted MS model linked with a subject-specific FRPVE FE model [15], both with 1 DoF knee joint MS models can predict the JCF comparable with experiments. Importantly, Andersen (2018) has shown that the inclusion of the subject-specific geometry does not improve the JCF predictions compared to a linearly-scaled MS model [32].

Therefore, the aims of the current study were twofold. First, we developed three different MS models with different levels of complexity. The first MS model consisted of an embedded 12 DoFs subject-specific knee with an elastic foundation model. The next two MS models were conventional models, one with a static-optimization MS model (Gait2392 MS Model) and the other an EMG-assisted MS model. Both of these used a 1 DoF knee joint with generic joint geometries. Our second aim was to use outputs from the three MS models to drive a muscle force driven FRPVE FE model (forward dynamics). We investigated whether the FRPVE FE model driven by a simpler MS model would suffice to simulate the knee joint compared to the MS model with an embedded 12 DoFs knee. We hypothesized that the embedded MS model (i.e. with a 12 DoFs knee joint) would outperform other modeling approaches due to considering soft tissue deformation as well as knee secondary kinematics (ligament interaction) while estimating muscle forces.

II. Methods

A. Workflow and Data Collection

The workflow of the current study is illustrated in Fig. 1 (see supplementary material, Fig. S1 for a more detailed workflow). One healthy subject (male, 78 kg, 1.77 m, and 33 years old) was recruited in our previous study [15] and was provided with a written informed consent. Briefly, ten level walking trials at the preferred speed were recorded in the gait analysis laboratory of the Faculty of Sport and Health Sciences, University of Jyväskylä. For each trial, synchronized marker trajectories (120 Hz sampling frequency, MX system, Vicon, UK), ground reaction forces (GRFs, 1200 Hz, two force plates, OR6-6, AMTI, USA), and EMG signals (1200 Hz, Telemyo 2400T-G2, Noraxon, USA) were collected. EMG signals were measured from vastus lateralis, rectus femoris, long head of biceps femoris, semitendinosus, medial gastrocnemius, soleus, and gluteus maximus during walking. The best trial among all the recorded trials (in terms of the least missed markers, the best quality of the EMGs and GRFs, etc.) was selected to drive the models. More information on data collection and data processing (e.g. EMG and GRF) are presented in our previous study [15] and in the supplementary material.

In addition to the gait data, MR images of the subject were taken in our previous study [33] (3.0 T scanner, Philips, Best, Netherlands) using a 3D fast spin-echo sequence (VISTA) to extract the subject-specific joint geometries. Segmentation was done manually in MIMICS v.15.01 (Materialise, Leuven, Belgium) and consisted of the knee joint cartilages (femoral, tibial, and patellar), menisci, ligament insertion points, and patellar tendons and ligaments [34]. The data collection was done with the permission (94/2011) from the local ethical committee of the Kuopio University Hospital, Kuopio, Finland.

B. MS Model

Three MS models with different levels of complexity were used in this study. The first MS model had a 12 DoFs knee joint model with an embedded elastic foundation model, while

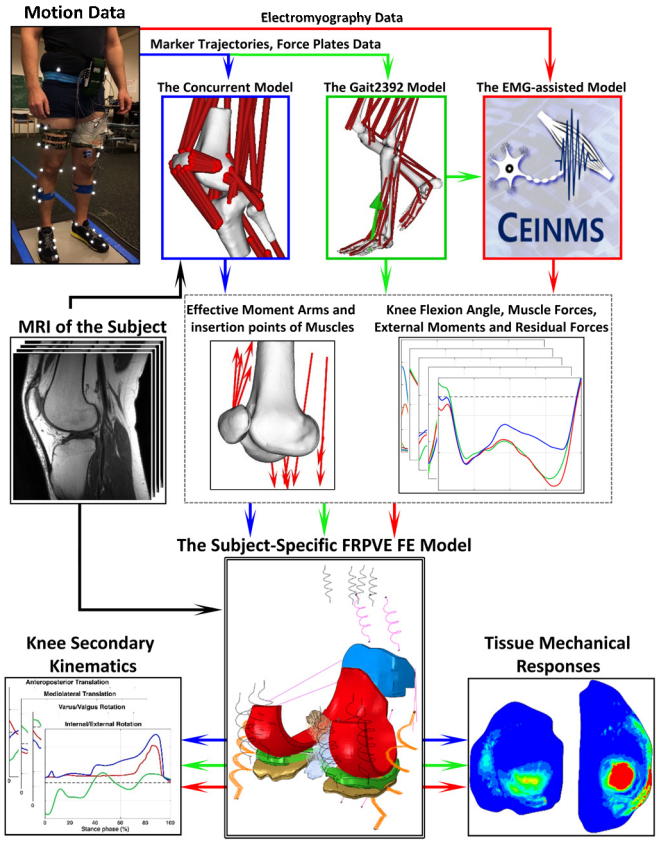

Fig. 1. The workflow of the study. A more detailed workflow is presented and discussed in the supplementary material (section 1.2.3 and Figs S1-S7).

the other two MS models had simpler 1 DoF knee models (see Table I). All muscle forces from the MS models were used as inputs to the FE model. Detailed explanations of the three MS and FE models, as well as model consistency considerations, are presented in the following subsections, Table I, and supplementary material.

1) The MS Model With the 12 DoFs Knee Joint: A previously developed and validated MS model with a 12 DoFs knee joint was used in the current study [20]. The first OpenSim release of the model (OpenSim Joint and Articular Mechanics) is freely available on the SimTK website. The knee joint consisted of a 6 DoFs tibiofemoral joint and a 6 DoFs patellofemoral joint. The subject-specific knee joint surfaces (explained in section II.A) consisting of femoral, tibial, and patellar cartilages were imported to the knee joint of the MS model. The contact pressures within the joint cartilages were calculated using a non-linear elastic foundation model [35], [36]. An elastic modulus of 20 MPa and a Poisson's ratio of 0.49 were considered for cartilages since it is shown to be capable of replicating contact pressures estimated by the use of the FRPVE material model [26].

Anteriomedial and posteriolateral anterior cruciate ligaments (aACL, pACL), anteriolateral and posteriomedial posterior cruciate ligaments (aPCL, pPCL), superficial and deep medial collateral ligaments (small, dMCL), lateral collateral ligament (LCL), patellar tendon, medial and lateral patellofemoral ligaments (MPFL, LPFL), popliteofibular ligament (PFL), posteriomedial capsule, posterior capsule, and the iliotibial band were included according to MRIs and modeled as non-linear spring bundles [20].

The aforementioned knee joint model was then embedded into a generic lower limb MS model [37]. The model included 43 muscles, a 3 DoFs ball-in-socket hip joint, the 12 DoFs knee joint, and a 1 DoF ankle joint. The geometry (except the subject-specific knee joint surfaces), mass and inertial properties as well as muscle properties which depend on length (e.g. optimal fiber length and tendon slack length) of the MS model were scaled based on the static trial of the subject. The static trial was captured while the subject stood still on the force plates and looked forward.

The whole model was implemented and analyzed in the Dynamics Pipeline of the SIMM (Software for Interactive Musculoskeletal Modeling, Musculographics Inc., Santa Rosa, CA) [38]. The muscle forces were estimated using a concurrent optimization. The optimization was performed to minimize the weighted sum of 1) squared muscle activations, 2) accelerations of the knee secondary kinematics, and 3) the contact energy of knee cartilages [20]. As only the knee flexion angle was used in the optimization, joint kinematics in the secondary knee DoFs evolved as a function of muscle, ligament, and contact forces [20], [36], [39].

2) The Standard Gait2392 MS Model: The second MS model of the study was developed using the standard Gait2392 MS model of the OpenSim software (v.3.3, SimTK) [9] in which the knee is modeled as a 1 DoF joint. Typically, this MS model does not incorporate subject-specific joint geometries and muscle activations are calculated utilizing a static-optimization method. The body segments, as well as muscle properties (e.g. tendon slack length and optimal fiber length), were linearly scaled based on the static trial of the subject. Then the static-optimization toolbox of the OpenSim software was employed to estimate muscle forces. Finally, the analysis toolbox of the OpenSim software was used to calculate inputs to the subject-specific FRPVE FE model (see section II.C.2).

3) The EMG-Assisted MS Model: The third MS model of the study was an EMG-assisted MS model with a 1 DoF knee joint utilizing the Calibrated EMG-Informed Neuromusculoskeletal Modelling Toolbox (CEINMS) [40]. We replaced the EMG-assisted CMC toolbox of OpenSim utilized in our previous study [15] with the CEINMS, since CEINMS provides different tendon models and various optimization functions for model calibration as well as muscle force estimation. Inputs to the CEINMS consisted of 1) external joint moments (from inverse dynamic analysis in OpenSim), 2) muscle moment arms and muscle-tendon length (extracted from the muscle analysis module of OpenSim), and 3) the EMG linear envelopes of the muscles of interest.

To keep the second and the third models more consistent, we used the second MS model of the study (the Gait2392) to provide the CEINMS with the aforementioned inputs. The muscle properties including maximum isometric force, pennation angle, tendon slack length, and optimal fiber length of the muscles were imported from the second MS model of the study to the CEINMS toolbox to calibrate the muscle-tendon parameters, accordingly. The hip joint (3 DoFs), knee joint (1 DoF), and ankle joint (1 DoF) were used to calibrate

TABLE I
DESCRIPTION OF THE THREE MSFE MODELS OF THE STUDY.

The MS model	The 12 DoFs knee MS model	The Gait 2392 MS model	The EMG-informed MS model
DOFs of the knee	12 DoFs	1 DoF	1 DoF
Geometries	Subject-specific knee joint surfaces, linear scaling for the rest of the model	Linear scaling	Linear scaling
Ligaments in the MS model	Ligaments were modeled as non-linear spring bundles, subject-specific insertion pints for ACL, PCL, LCL, and MCL	No ligaments	No ligaments
Tissue material models	Elastic foundation with non-linear contact pressure model	Solid segments	Solid segments
Muscle force estimation algorithm	Static-optimization to minimize the contact energy and to induce zero acceleration of the secondary kinematics	Static-optimization	Hybrid (EMG-informed and static-optimization alongside)
Outputs of the MS models (as inputs) to the FRPVE FE model	Knee flexion angle, muscle forces, muscle insertion points, line of action of muscles, external joint moments, residual JCF		
FE model DOFs	5 unconstrained DoFs on the femur (the knee flexion angle was used as input), 6 unconstrained DoFs on the patella		
Outputs from the FE model	Knee secondary kinematics, knee JCF, contact area, tissue mechanical responses (stress, strain, fluid pressure, etc.)		

muscle-tendon parameters of 43 muscles of the leg of the interest. Three walking trials (different than the selected trial for the workflow) were used for calibration. The multi-DoFs calibration was performed to adjust the muscle-tendon parameters while minimizing the error between measured joint moments and moments estimated by the model [40], [41].

Following calibration, the hybrid mode of the CEINMS toolbox was used to implement the EMG-assisted analysis. Similar to calibration, 5 DoFs, as well as 43 muscles of the leg of the interest, were used in the execution of the EMG-assisted MS model. Using the inputs of muscle-tendon moment arms and lengths, EMG linear envelopes and external joint moments estimated by inverse dynamics, the EMG-assisted model estimated muscle excitations by adjusting EMG linear envelopes and synthesizing excitations without EMGs. This was performed using static-optimization that minimized the weighted sum of the: 1) square of the error between the external moments and the internal moments generated by muscles, 2) square error of the estimated muscles' excitations and EMG linear envelopes, and 3) square of the estimated muscles' excitations. This optimization performed using simulated annealing to help avoid local minima. Tendons were considered as elastic elements.

In summary, all three MS models were driven with the same gait kinematics and kinetics. Finally, the knee flexion angle, as well as three sets of estimated muscle forces, muscle insertion points, net joint moments, and the residual JCF were estimated by the MS models (inverse dynamics) to drive (forward dynamics) the FRPVE FE model. These quantities are explained in more detail in section II.C.2.

C. The FE Model Incorporating FRPVE Material Properties

1) Geometry, Material Properties, and Model Consistency:

The muscle force driven FRPVE FE model exploited our previously developed and validated model [15], [34]. Femoral, tibial, and patellar cartilages were modeled as a FRPVE material [42]–[44] with split-lines and the depth-dependent Benninghoff-type arcade architecture of primary collagen fibrils [45]–[48]. The menisci were modeled as a fibril-reinforced poroelastic (FRPE) material with circumferentially oriented collagen fibrils [34], [49]. Meniscal horn attachments were modeled as linear spring bundles [50]. Knee joint ligaments including ACL, PCL, MCL, and LCL were modeled as non-linear spring bundles with slack, toe, and linear regions. Pre-strains and stiffness of the ligaments were set according to the literature [51] similar to the 12 DoFs knee MS model of the study (see section II.B.1). The secondary kinematics estimated by the FE model driven by the results of the 12 DoFs knee MS model (see section II.C.2) and the secondary kinematics estimated directly by the 12 DoFs knee MS model were compared as a validation of the consistency between FE and MS models (Fig. S3). A detailed description of the material models, material parameters, and model implementation are presented in the supplementary material.

2) Inputs and Boundary Conditions of the FRPVE FE Model:

The three MS models were used to obtain three sets of inputs to drive the FRPVE FE model. Outputs from the MS models consisted of the 1) knee flexion angle (inverse kinematics), 2) net external joint moments (inverse dynamics), 3) muscle forces, 4) residual JCF on the knee joint, 5) muscle effective moment arms (lines of action), and 6) muscle insertion points [52]. All the quantities were transformed into the local coordinate system fixed to the proximal tibia to represent the motion of the femur relative to the tibia. Consequently, all the tibial nodes located on the bone-cartilage interface were fixed in all directions (encastre) and knee flexion angle and well as joint moments and the residual JCF on the knee joint were applied on the reference point of the femur.

The reference point of the femoral cartilage was defined in the middle of the medial and lateral femoral epicondyles. All the femoral cartilage nodes on the bone-cartilage interface were coupled to this reference point. The knee flexion angle was applied to the reference point of the femur to force the FE model to follow the primary kinematics while the other 5 DoFs (secondary kinematics) of the femur were unconstrained and free to move. Patella was unconstrained and free in all its 6 DoFs and it was positioned according to the quadriceps force, patellar tendon, MPFL, and LPFL, and movements of the femur.

Eleven muscles were added around the knee joint in the FRPVE FE model. These consisted of the quadriceps muscles

(rectus femoris, vastus lateralis, vastus intermedius, and vastus medialis), hamstrings (semimembranosus, semitendinosus, and biceps femoris short head and long head), medial and lateral gastrocnemius, and gracilis. Muscle insertion points were calculated from each MS model separately using a previously developed plug-in of the OpenSim software [52] and then imported to the FE models, accordingly. One end of each muscle was coupled to the reference point of the femur based on the calculated muscle insertion points and the other end was set free to apply the corresponding 3D vector of muscle forces as estimated by the MS models. Consequently, muscle force directions and moment arms were adjusted according to the forces.

Net joint moments (internal-external and varus-valgus moments) were calculated using the MS models in OpenSim (inverse dynamics) and were applied to the femoral reference point. These external moments were counterbalanced by the moments generated by the muscles and the passive force of ligaments (Fig. S4). Finally, the residual JCF passing through the knee joint (Fig. S6) was calculated by subtracting muscle forces and ligament forces from the total knee JCF (ligament forces were available only in the MS model with the 12 DOFs knee joint). This residual JCF (anteroposterior, mediolateral, and vertical directions) was applied to the femoral reference point in each corresponding FE model (Fig. S6). Detailed explanations of the residual JCF is presented in the supplementary material as well as our previous work [15].

It should be noted that an excessive and physiologically unrealistic external rotation of the femur was observed in the FE simulation (more than 30 degrees) when imposing the results of the static-optimization based Gait2392 MS model of the study. Therefore, we used the internal-external rotation of the femur as an extra boundary condition in the FE model when driven by the Gait2392 MS model (Fig. 2B, the green line). The internal-external rotation of the femur was obtained from the inverse kinematics of the gait trial of the subject.

The initial conditions of the FRPVE FE models were set to represent the situation at the heel strike of the left leg and the whole stance phase of the left leg was analyzed in Abaqus software (Dassault Systèmes, United States).

3) Analysis of the Contact Area and Tissue Mechanical Responses: The contact area was defined as 4 contact regions on the tibial cartilage recognized by non-zero nodal contact pressures (consisted of tibia-to-femur and tibia-to-menisci contact regions). The four contact regions consisted of: 1) femoral-cartilage to medial-tibial-cartilage, 2) medial-meniscus to medial-tibial-cartilage, 3) femoral-cartilage to lateral-tibial-cartilage, and 4) lateral-meniscus to lateral-tibial-cartilage. Finally, the total contact area and the contact area ratio were calculated using the area of the four contact regions.

The distributions of the tissue mechanical responses at the peak of the JCFs of each MSFE model were analyzed. In addition, the average as well as the mean of the upper quartile of the tissue mechanical responses over the tibial contact area were calculated. We chose the mean of the upper quartile (instead of i.e. maximum) to place more weight on the maximum values, as well as reducing the effect of possible outliers (abrupt results due to highly non-linear material model or node-dependent outliers).

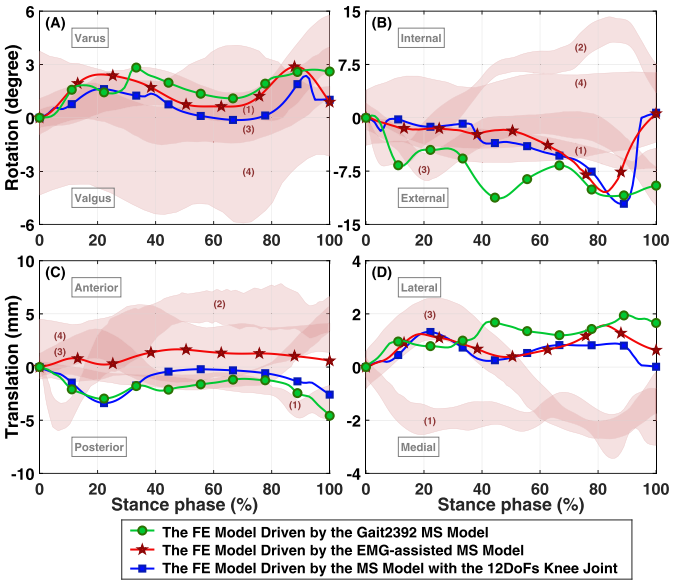

Fig. 2. Secondary knee kinematics (femur relative to the tibia) compared with experiments; (A) varus-valgus rotation, (B) internal-external rotation, (C) anteroposterior translation, and (D) mediolateral translation. All the graphs are shifted to start from zero for ease of comparison and to exclude differences in the coordinate systems. Note that the results from previous studies are transformed to be represented in the same coordinate system of our study.

To calculate the average of tissue mechanical responses, first all the nodes of the tibial cartilage in contact with either femoral cartilage or menisci were selected at each time point of the gait cycle. Then the sum of nodal values of the parameter of interest was calculated and divided by the number of nodes in the contact area for that time increment.

The mean of the upper quartile of tissue mechanical responses was calculated by sorting all the nodal values on the tibial cartilage in descending order, separately at each time point. Only the tibial nodes which were in contact with either femoral cartilage or menisci were chosen. Then the first 25 % of the data was selected at each time point. Finally, the average of the selected data (at each time point) was calculated and plotted against the stance phase.

III. Results

A. Knee Joint Kinematics and Kinetics

The experimental secondary kinematics of the knee joint obtained from the literature [53]–[56] show noticeable subject related as well as measurement-method related variations in patterns and magnitudes (Fig.2). However, the estimated varus-valgus and internal-external rotations, as well as anterior-posterior translations by all the MSFE models, were favorably comparable with experiments (Fig. 2). The medio-lateral translation estimated by the three MSFE models had similar patterns and magnitudes; however, there were discrepancies in the pattern of the mediolateral translation between experiments and those estimated by simulations (Fig. 2D).

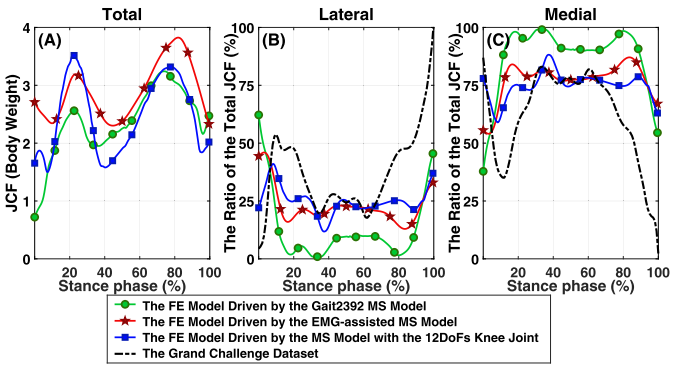

Fig. 3. Estimated JCF compared with the first two Grand Challenge Dataset; (A) total JCF, (B) normalized lateral JCF, and (C) normalized medial JCF.

The maximum JCF varied from 3.25 to 3.8 bodyweight estimated by the three MSFE models. However, the EMG-assisted and the 12 DoFs knee MSFE models estimated similar normalized mediolateral JCFs favorably comparable to experiments [7], compared to the JCF estimated by the Gait2392 MSFE model (Fig. 3B and 3C). In the standard Gait2392 MSFE model, a continuous joint contact was not achieved during the entire stance phase in the lateral compartment (the JCF was almost zero for up to 8% stance) (Fig. 3B). The root mean square deviation (RMSD) between the average of the normalized lateral JCF from the Grand Challenge Dataset and the normalized lateral JCF predicted by the Gait 2392, EMG-assisted, and the 12 DoFs knee MSFE models were 35.3, 24.6, and 19.95, respectively (Fig. 3B). The corresponding RMSDs on the medial joint compartment were 32.3, 25.5, and 21.6 for the Gait 2392, EMG-assisted, and the 12 DoFs knee MSFE models, respectively (Fig. 3C).

B. The Center of Pressure and the Contact Area on the Knee

The COP trajectories on the medial tibial cartilage were similar between the three MSFE models (Fig. 4). However, there were apparent differences on the lateral side. On the medial tibial cartilage, COP passed through the menisci for up to 68%, 31%, and 75% of the stance phase compared to 80%, 20%, and 41% on the lateral side, estimated by the Gait2392, the EMG-assisted, and the 12 DoFs knee MSFE models, respectively (Fig. 4). In other words, the COP located mostly under menisci in the Gait2392 model, while it passed mostly through cartilages in the EMG-assisted model.

The whole contact area on the lateral side estimated by the standard Gait2392 MSFE model was located only under the meniscus for more than 60% of the stance phase (Fig. 5). In contrast, the lateral contact area was distributed between the menisci and cartilage during the whole stance phase in both EMG-assisted and 12 DoFs knee MSFE models. The lateral cartilage-to-menisci contact area ratio was 0.10±0.25, 0.94±0.24, and 0.58±0.20 estimated by the Gait2392, the EMG-assisted, and the embedded MSFE models respectively, compared to 0.46±0.067 from *in situ* measurements [53] (Fig. 5C). The estimated contact area at the medial side was similar between the MS models and experimental data. The

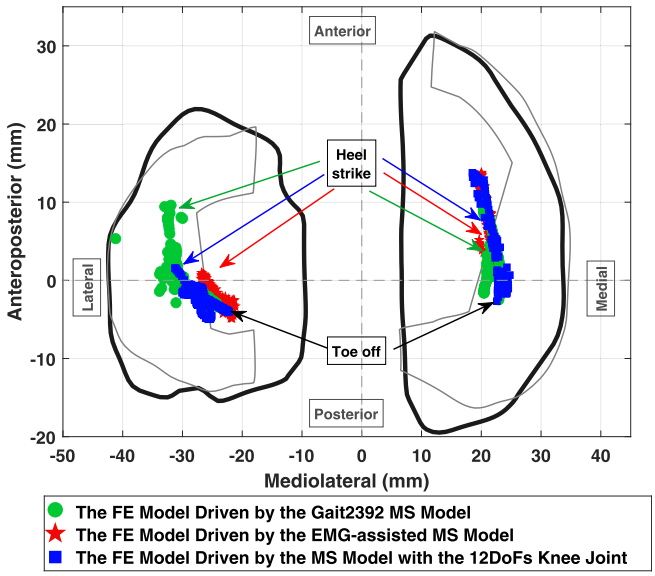

Fig. 4. The COP of the compressive force applied to the medial and lateral compartments of the tibial cartilage for the three MSFE models.

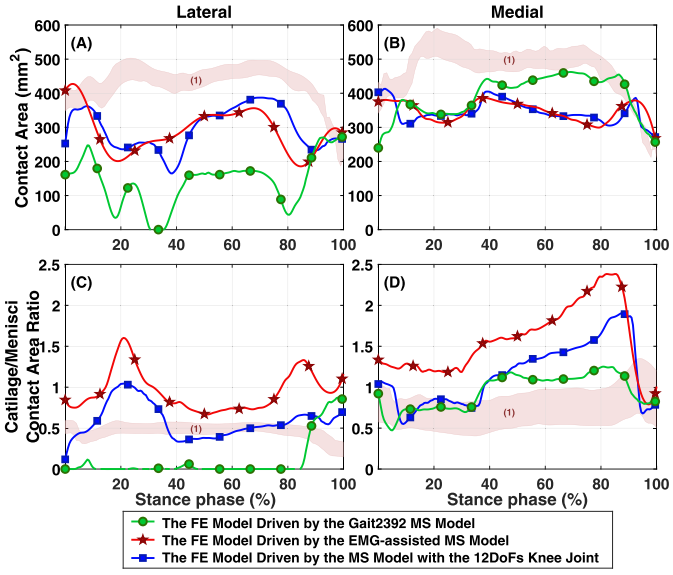

(1) Experimental data [53]

Fig. 5. Contact area of the knee joint; (A) total lateral contact area, (B) total medial contact area, (C) cartilage-to-cartilage/menisci-to-cartilage contact area ratio on the lateral tibial plateau, and (D) cartilage-to-cartilage/menisci-to-cartilage contact area ratio on the medial tibial plateau.

cartilage-to-menisci contact area ratio was 0.74±0.1 for the *in situ* measurements [53], 0.95±0.21 for the Gait2392 MSFE model, 1.57±0.42 for the EMG-assisted MSFE model, and 1.16±0.38 for the 12 DoFs knee MSFE model (Fig. 5D).

C. Cartilage Mechanical Response

The average (Fig. 6), the distribution (Fig. 7), as well as the mean of the upper quartile of the tissue mechanical responses (Fig. S9), were estimated fairly similar by all the three MSFE models on the medial tibial cartilage. On the lateral tibial cartilage, in contrast, the Gait2392 MSFE model estimated different tissue mechanical responses compared to the other two MSFE models (Figs. 6, 7, and S9-S11). The maximum

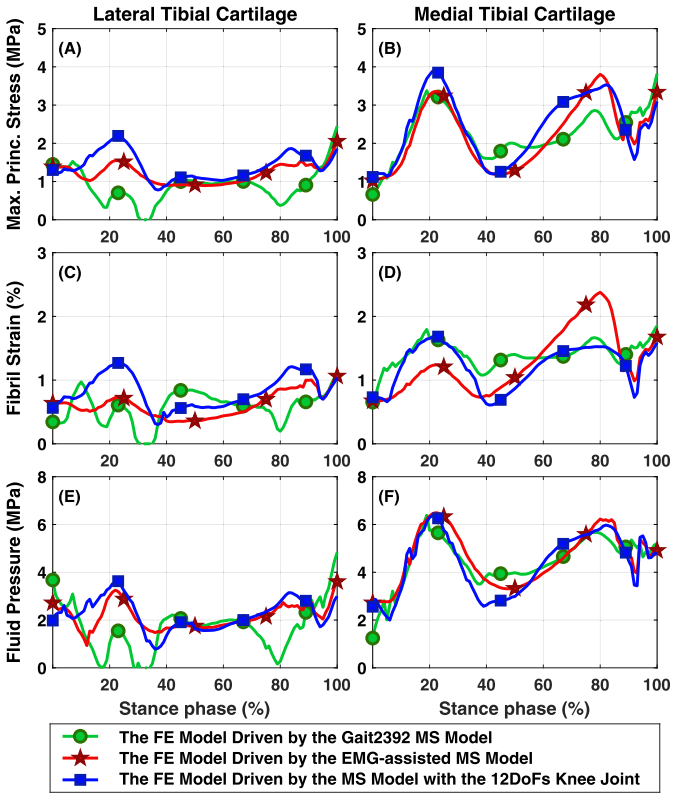

Fig. 6. Average of the (A) lateral maximum principal stress, (B) medial maximum principal stress, (C) lateral collagen fibril strain, (D) medial collagen fibril strain, (E) lateral fluid pressure, and (F) medial fluid pressure on the tibial cartilage contact area.

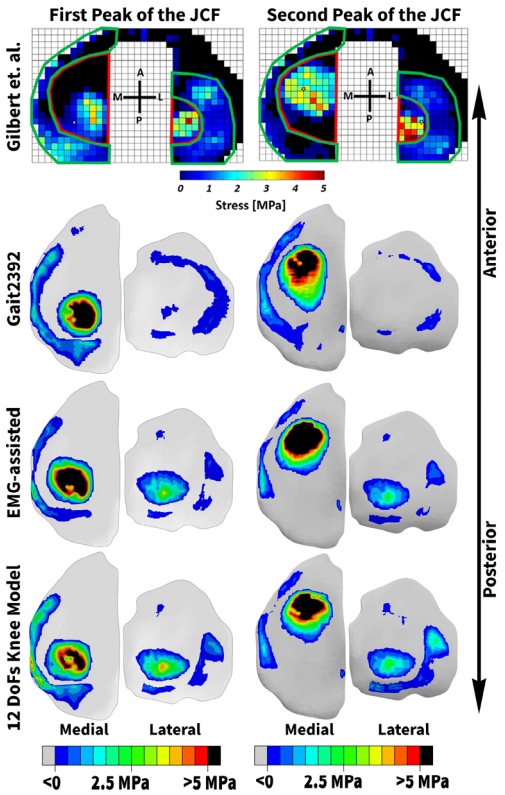

Fig. 7. The experimental contact pressure [53] (top row, used with permission) compared to the contact pressure estimated by the three MSFE models of the study.

principal stress, fibril strain, and fluid pressure estimated by the EMG-assisted and the 12 DoFs knee MSFE models reached the maximum at the first and second peaks of the GRF on the lateral side. In contrast, the Gait2392 MSFE model predicted minimum tissue mechanical responses of the lateral tibial cartilage at the first and second peaks of the GRF (Figs. 6, 7, and S9-S11).

Both the magnitude and the distribution (the mediolateral-anteroposterior, as well as the menisci-to-cartilage distributions) of the contact pressure (Fig. 7) estimated by the EMG-assisted MSFE model and the 12 DoFs MSFE model were consistent with experiments [53], [57], while the Gait2392 MSFE model estimated considerably lower contact pressure on the lateral tibial cartilage.

IV. Discussion

A. Summary

In this study, a subject-specific 12 DoFs multiscale MSFE model of the knee joint was developed and compared with experimental literature data. The MS model component included a 12 DOFs knee joint with subject-specific geometries, an embedded (concurrent) elastic foundation model of cartilages, and nonlinear elastic ligaments, which provided muscle force inputs for a muscle force-driven FE model with identical geometries and boundary conditions. In the FE model component, cartilage and menisci were modeled as highly detailed FRPVE and FRPE materials, respectively. A key advantage of the employed MS model is that the muscle force estimation is conducted considering the knee secondary kinematics, cartilage deformations and contact pressure, and ligament forces which all alter muscle forces [18].

The second advantage of the approach is that the muscle-force driven FE model uses state-of-the-art material models for cartilage and menisci enabling an analysis of e.g. fibril strain and fluid pressure within these tissues. These properties are known to play a vital role in governing degradative and adaptive responses of these tissues [4], [5], [24]. To the best of our knowledge, none of the previous studies have integrated all the aforementioned capabilities into a single modeling framework. We also assessed the 12 DoFs knee MSFE model against two more conventional rigid-body MS models; the standard Gait2392 MS model (OpenSim) and an EMG-assisted MS model (CEINMS toolbox), for which we sequentially first solved the MS and then the FE models. It was shown that the FE model driven by the MS model with a 12 DoFs knee and fairly the FE model driven by the EMG-assisted MS model produced results that better replicate the literature-based experimental studies, compared to the FE model driven by the Gait2392 MS model.

B. Kinematics and Kinetics

The internal-external rotations, the varus-valgus rotations, and the anteroposterior translations estimated by the three MSFE models were favorably comparable with experiments (Fig. 2). The estimated resultant muscle forces (Fig. S7) were mostly toward the medial side of the knee, which could be the reason for the inconsistency of the mediolateral translation

between experiments and those estimated by the MSFE models of our study (Fig. 2D). It should be noticed that the FE model was not driven using the resultant internal-external rotation moment estimated by the static-optimization based Gait2392 MS model. This was due to excessive external rotation of the femur from early to mid-stance, caused by the external rotation moments generated by the estimated muscle forces (Fig. S4-B, the green dashed line). Thereby, the 12 DoFs knee and the EMG-assisted MSFE models show promises to be used in secondary kinematics analyses, e.g. gait modification methods, rehabilitation exercises, knee orthoses and prosthetics, and knee osteotomy surgery which all try to redistribute the knee joint loading by re-aligning the joint.

Resultant muscle forces estimated by the 12 DoFs knee MS model were less than those estimated by the Gait2392 and EMG-assisted MS models. However, the estimated total JCF by the FE models were slightly higher for the 12 DoFs knee MSFE model (Fig. 3). This was due to higher resultant internal-external moment (Fig.S4) that was compensated by the passive ligament forces. Consequently, estimated ligament forces were different in the three MSFE models (Fig. S8). Thus, the modeling approach affects ligament force predictions which are important for example in studies investigating ACL rupture and reconstruction.

Numerous studies have been conducted to investigate the mediolateral distribution of the JCF under different activities or conditions. Most of the approaches have predicted considerably lower JCF on the lateral compartment of the knee joint compared to experimental findings [2], [30], [32], [58]. Similar to those studies, the Gait2392 MSFE model of the study predicted the lowest lateral JCF compared to the other two MSFE models, as well as the Grand Challenge Dataset (Fig. 3). Consistent with previous studies [59]–[63], the use of the EMG-informed MS model improved agreement of the mediolateral distribution of the JCF with the experimental data. Contribution of the estimated muscle forces to the medial and lateral JCF can be seen in Fig. S4-A (i.e. the varus-valgus moment generated by muscles). Nonetheless, the medial and lateral JCF estimated by the 12 DoFs knee and the EMG-assisted MSFE models showed the best agreement with the Grand Challenge Dataset in terms of the patterns and magnitudes (Fig. 3).

C. Center of Pressure and Contact Area

Although it is important to be able to estimate the magnitude of the mechanical responses accurately within soft tissues (such as the JCF, stress, strain, and fluid pressure), the accuracy of the distribution of each of those responses over the joint surfaces might be even more crucial. Inaccurate estimation of the location of the tissue responses (stress, strain, fluid pressure, etc.) could influence studies focusing on the prediction of cartilage degeneration [4], [57], [64]. To our knowledge, this is the first study that reports both the COP on the knee joint (including the effect of the menisci) and the contact area for the whole stance phase of the gait and compares those to experimental findings (Figs. 4 and 5). All the three MSFE models of the study estimated comparable medial contact area (Fig. 5B). However, the lateral contact area (Fig. 5A) estimated by the 12 DoFs knee MSFE and EMG-assisted MSFE models agreed better with the experimental findings [53], [65] than the Gait2392 MSFE model. Considering both the lateral and medial sides, the 12 DoFs knee MSFE model estimated cartilage-to-menisci contact area ratio (both the patterns and magnitudes) more consistent with experimental values [53], compared to those estimated by the EMG-assisted and Gait2392 MSFE models (Figs. 5C and 5D).

D. Cartilage Mechanical Responses

Unfortunately, no experimental data is available to compare with estimated stress, fibril strain, and fluid pressure within the cartilage. However, the estimated results by the EMG-assisted and the 12 DoFs knee MSFE models of the study (and those estimated by the Gait2392 MSFE model on the medial tibial cartilage) were comparable with previous numerical studies [2], [14], [33], [34], [64]. Particularly, excessive maximum principal stress and different strain definitions within cartilage, such as fibril strain, have been suggested as distinct biomechanical markers for cartilage degradation. Consequently, they have been applied in simulations to trigger the progression of OA [4], [5], [24], [25], [66]. According to our results (Figs. 6, 7, and S9-S11), we think that the new modeling approach could potentially improve the estimated tissue mechanical responses and consequently, may affect the prediction of time-dependent tissue degeneration.

E. Limitations

One limitation of the current study is the use of one participant. However, the focus of the study was on the development of a new method. Besides, comparisons were made based on the relative and normalized values instead of the magnitudes. Moreover, the utilized models in this study have been compared, optimized, and validated with the experiments [20], [31], [67], [68]. Nonetheless, we would evaluate the presented workflow utilizing numerous subjects performing different daily activities and rehabilitation exercises in our future studies. No experimental data are available to compare with the tissue mechanical responses such as stress, fibril strain, and fluid pressure; however, they were comparable with previous studies based on numerical modeling [2], [14], [33], [34], [64]. Currently, there are no methods to fully extract subject-specific mechanical properties of soft tissues such as cartilages, menisci, and ligaments which might affect the results [6], [69]. Therefore, literature-based material properties were implemented in all soft tissues and kept them identical in all MSFE models. Moreover, the developed 12 DoFs knee MSFE model estimations did not utilize EMG signals (i.e. the model was not EMG assisted) in the estimation of muscle forces which might be a limitation of the study; however, this model outperforms the other two.

V. Conclusion

To conclude, we developed a subject-specific MSFE model with a 12 DoFs knee joint. The performance of the model

was compared with experimental data and previous MSFE model implementations. Our research aimed to answer the question of which MS modeling approach would be most appropriate to be used in conjunction with a FRPVE FE model. Assisting the muscle force estimations with EMG signals while keeping the joint simple, or just including the secondary kinematics as well as the soft tissue deformations and utilizing an optimization-based muscle force redundancy solver. In addition, we wanted to investigate whether the simplest MS model (1 DoF knee and static-optimization based muscle force estimation) would suffice.

In general, the EMG-assisted and 12 DoFs knee MS models produced comparable magnitudes and patterns in their resultant varus-valgus and internal-external rotation knee moments (Fig. S4), the muscle forces (Figs. S5 and S7), the residual JCF (Fig. S6), and the total JCF, as well as the mediolateral JCF distribution (Fig. S2). However, these two MS models' outputs were different to those from the Gait2392 MS model. There are a few reasons for the similar, although not identical, results from the EMG-assisted and 12 DoFs knee MS models. The 12 DoFs knee MS model incorporated the knee varus-valgus and internal-external rotation moments to adjust and estimate the secondary knee kinematics, which altered the muscle moment arms and ligament passive forces to achieve dynamic equilibrium. On the other hand, the EMG-assisted MS model was first informed by EMGs, which are directed to stabilize knee varus-valgus moments [70], [71], and second calibrated and executed on multi-DoFs using lower limb external moments on the joints to achieve dynamic equilibrium [41]. In contrast, the muscle forces estimated by static-optimization based MS model was not informed by the knee varus-valgus moments, internal-external rotation moments, nor EMGs.

Although there were differences between the outputs estimated by the three MS models, their (dis)similarities mapped into the loading and boundary conditions of FE models, which by virtue incorporated interactions between knee moments, muscle forces, and knee ligaments to achieve quasi-static equilibrium and had corresponding influences on the FE models' results. For instance, the large knee external rotation moments in early to mid-stance from the Gait2392 MS model (Fig. S4) translated to excessive external femoral rotation in its associated FE model (Fig. 2). Furthermore, and in general, having the varus-valgus DoF in the FE model biased the JCF towards the medial side with low lateral JCF in the static-optimization MSFE models. However, more physiologically plausible muscle forces and medial and lateral JCF forces came from the EMG-assisted and 12 DoFs knee MS models, which produced more consistent and plausible results in both their corresponding FE models (Fig. 3, Fig. 7, Fig. S2, Fig. S4).

Nevertheless, the FE model driven by the MS model with the 12 DoFs knee joint bore a closer resemblance to experimental JCF, contact area, and tissue mechanical responses, compared to the EMG-assisted MSFE model. On the other hand, the creation of the 12 DoFs knee MS model requires considerable effort (including segmentation and assembly of the model) and the MS model takes a considerable time to run. These could be considered a limitation with its clinical use. However, our future study is focused on the development of a 12 DoFs EMG-assisted MSFE model firstly to evaluate if considering the EMGs could improve muscle force estimations as well as the secondary kinematics, and secondly to decrease the model creation and runtime utilizing e.g. machine learning [72].

We think that the developed method could be used in a wide range of studies including analyzes of different activities and gait modifications, predict outcomes of different surgeries (such as knee osteotomy, ACL reconstruction, and total knee replacement), and simulate adaptation of soft tissues such as cartilages or ligaments. Nonetheless, currently the EMG-assisted MSFE approach might be the preference as a rapid clinical assessment tool.

Appendix

More information on the method and results are presented in the supplementary material.

Acknowledgment

CSC–IT Center for Science Ltd, Finland, is acknowledged for providing FE software. The authors gratefully acknowledge the Faculty of Sport and Health Sciences, University of Jyväskylä, Finland for providing the laboratory facilities for the experimental measurements. The authors also acknowledge the help of Dr. P. Vartiainen and Dr. C. R. Smith.

References

[1] A. J. Baliunas *et al.*, "Increased knee joint loads during walking are present in subjects with knee osteoarthritis," *Osteoarthritis Cartilage*, vol. 10, no. 7, pp. 573–579, Jul. 2002.

[2] K. S. Halonen, C. M. Dzialo, M. Mannisi, M. S. Venäläinen, M. De Zee, and M. S. Andersen, "Workflow assessing the effect of gait alterations on stresses in the medial tibial cartilage—Combined musculoskeletal modelling and finite element analysis," *Sci. Rep.*, vol. 7, no. 1, pp. 1–14, 2017.

[3] T. Miyazaki, M. Wada, H. Kawahara, M. Sato, H. Baba, and S. Shimada, "Dynamic load at baseline can predict radiographic disease progression in medial compartment knee osteoarthritis," *Ann. Rheumartic Disease*, vol. 61, no. 7, pp. 617–622, Jul. 2002.

[4] M. K. Liukkonen, M. E. Mononen, O. Klets, J. P. Arokoski, S. Saarakkala, and R. K. Korhonen, "Simulation of subject-specific progression of knee osteoarthritis and comparison to experimental follow-up data: Data from the osteoarthritis initiative," *Sci. Rep.*, vol. 7, no. 1, p. 9177, Dec. 2017.

[5] W. Wilson, C. van Burken, C. C. van Donkelaar, P. Buma, B. van Rietbergen, and R. Huiskes, "Causes of mechanically induced collagen damage in articular cartilage," *J. Orthopaedic Res.*, vol. 24, no. 2, pp. 220–228, Dec. 2006.

[6] H. N. Beidokhti, D. Janssen, S. van de Groes, J. Hazrati, T. Van den Boogaard, and N. Verdonschot, "The influence of ligament modelling strategies on the predictive capability of finite element models of the human knee joint," *J. Biomech.*, vol. 65, pp. 1–11, Dec. 2017.

[7] B. J. Fregly *et al.*, "Grand challenge competition to predict *in vivo* knee loads," *J. Orthopaedic Res.*, vol. 30, no. 4, pp. 503–513, Apr. 2012.

[8] W. R. Taylor *et al.*, "A comprehensive assessment of the musculoskeletal system: The CAMS-knee data set," *J. Biomech.*, vol. 65, pp. 32–39, Dec. 2017.

[9] S. L. Delp *et al.*, "OpenSim: Open-source software to create and analyze dynamic simulations of movement," *IEEE Trans. Biomed. Eng.*, vol. 54, no. 11, pp. 1940–1950, Nov. 2007, doi: 10.1109/TBME.2007.901024.

[10] M. G. Pandy, "Computer modeling and simulation of human movement," *Annu. Rev. Biomed. Eng.*, vol. 3, no. 1, pp. 245–273, Aug, 2001.

[11] T. S. Buchanan, D. G. Lloyd, K. Manal, and T. F. Besier, "Neuromusculoskeletal modeling: Estimation of muscle forces and joint moments and movements from measurements of neural command," *J. Appl. Biomech.*, vol. 20, no. 4, pp. 367–395, Nov. 2004.

[12] D. G. Thelen and F. C. Anderson, "Using computed muscle control to generate forward dynamic simulations of human walking from experimental data," *J. Biomech.*, vol. 39, no. 6, pp. 1107–1115, 2006.

[13] D. I. Caruntu, "Knee joint modeling," in *Proc. 21st Biennial Conf. Mech. Vib. Noise*, vol. 1, 2007, pp. 673–678.

[14] H. Marouane, A. Shirazi-Adl, and M. Adouni, "3D active-passive response of human knee joint in gait is markedly altered when simulated as a planar 2D joint," *Biomech. Model. Mechanobiol.*, vol. 16, no. 2, pp. 693–703, 2017.

[15] A. Esrafilian, L. Stenroth, M. E. Mononen, P. Tanska, J. Avela, and R. K. Korhonen, "EMG-assisted muscle force driven finite element model of the knee joint with fibril-reinforced poroelastic cartilages and menisci," *Sci. Rep.*, vol. 10, no. 1, pp. 1–16, Feb. 2020.

[16] A. Navacchia, V. Kefala, and K. B. Shelburne, "Dependence of muscle moment arms on *in vivo* three-dimensional kinematics of the knee," *Ann. Biomed. Eng.*, vol. 45, no. 3, pp. 789–798, 2017.

[17] D. R. Hume, A. Navacchia, A. A. Ali, and K. B. Shelburne, "The interaction of muscle moment arm, knee laxity, and torque in a multi-scale musculoskeletal model of the lower limb," *J. Biomech.*, vol. 76, pp. 173–180, Jul. 2018.

[18] A. Navacchia, D. R. Hume, P. J. Rullkoetter, and K. B. Shelburne, "A computationally efficient strategy to estimate muscle forces in a finite element musculoskeletal model of the lower limb," *J. Biomech.*, vol. 84, pp. 94–102, Feb. 2019.

[19] A. A. Ali *et al.*, "Validation of predicted patellofemoral mechanics in a finite element model of the healthy and cruciate-deficient knee," *J. Biomech.*, vol. 49, no. 2, pp. 302–309, Jan. 2016.

[20] R. L. Lenhart, J. Kaiser, C. R. Smith, and D. G. Thelen, "Prediction and validation of load-dependent behavior of the tibiofemoral and patellofemoral joints during movement," *Ann. Biomed. Eng.*, vol. 43, no. 11, pp. 2675–2685, Nov. 2015.

[21] P. Julkunen, T. Harjula, J. Marjanen, H. J. Helminen, and J. S. Jurvelin, "Comparison of single-phase isotropic elastic and fibril-reinforced poroelastic models for indentation of rabbit articular cartilage," *J. Biomech.*, vol. 42, no. 5, pp. 652–656, Mar. 2009.

[22] N. Mukherjee and J. S. Wayne, "Load sharing between solid and fluid phases in articular cartilage: II—Comparison of experimental results and up finite element predictions," *J. Biomech. Eng.*, vol. 120, no. 5, p. 620, Oct. 1998.

[23] J. M. P. Quiroga, W. Wilson, K. Ito, and C. C. van Donkelaar, "Relative contribution of articular cartilage's constitutive components to load support depending on strain rate," *Biomech. Model. Mechanobiol.*, vol. 16, no. 1, pp. 151–158, Feb. 2017.

[24] J. T. Mäkelä, S.-K. Han, W. Herzog, and R. Korhonen, "Very early osteoarthritis changes sensitively fluid flow properties of articular cartilage," *J. Biomech.*, vol. 48, no. 12, pp. 3369–3376, Sep. 2015.

[25] L. P. Li and K. B. Gu, "Reconsideration on the use of elastic models to predict the instantaneous load response of the knee joint," *Proc. Inst. Mech. Eng. H, J. Eng. Med.*, vol. 225, no. 9, pp. 888–896, Sep. 2011.

[26] O. Klets, M. E. Mononen, P. Tanska, M. T. Nieminen, R. K. Korhonen, and S. Saarakkala, "Comparison of different material models of articular cartilage in 3D computational modeling of the knee: Data from the Osteoarthritis Initiative (OAI)," *J. Biomech.*, vol. 49, no. 16, pp. 3891–3900, Dec. 2016.

[27] A. Shirazi-Adl, "On the fibre composite material models of disc annulus—Comparison of predicted stresses," *J. Biomech.*, vol. 22, no. 4, pp. 357–365, Jan. 1989.

[28] J. C. Ihn, S. J. Kim, and I. H. Park, "*In vitro* study of contact area and pressure distribution in the human knee after partial and total meniscectomy," *Int. Orthopaedic*, vol. 17, no. 4, pp. 214–218, Aug. 1993.

[29] E. L. Radin, F. de Lamotte, and P. Maquet, "Role of the menisci in the distribution of stress in the knee," *Clin. Orthopaedic Related Res.*, vol. 185, pp. 290–294, May 1984.

[30] M. A. Marra *et al.*, "A subject-specific musculoskeletal modeling framework to predict *in vivo* mechanics of total knee arthroplasty," *J. Biomech. Eng.*, vol. 137, no. 2, p. 020904, 2015.

[31] P. Gerus *et al.*, "Subject-specific knee joint geometry improves predictions of medial tibiofemoral contact forces," *J. Biomech.*, vol. 46, no. 16, pp. 2778–2786, Nov. 2013.

[32] M. S. Andersen, "How sensitive are predicted muscle and knee contact forces to normalization factors and polynomial order in the muscle recruitment criterion formulation?" *Int. Biomech.*, vol. 5, no. 1, pp. 88–103, Jan. 2018.

[33] A. Kłodowski *et al.*, "Merge of motion analysis, multibody dynamics and finite element method for the subject-specific analysis of cartilage loading patterns during gait: Differences between rotation and moment-driven models of human knee joint," *Multibody Syst. Dyn.*, vol. 37, no. 3, pp. 271–290, Jul. 2016.

[34] K. S. Halonen *et al.*, "Importance of patella, quadriceps forces, and depthwise cartilage structure on knee joint motion and cartilage response during gait," *J. Biomech. Eng.*, vol. 138, no. 7, pp. 71002–71011, Jun. 2016.

[35] Y. Bei and B. J. Fregly, "Multibody dynamic simulation of knee contact mechanics," *Med. Eng. Phys.*, vol. 26, no. 9, pp. 777–789, Nov. 2004.

[36] D. G. Thelen, K. Won Choi, and A. M. Schmitz, "Co-simulation of neuromuscular dynamics and knee mechanics during human walking," *J. Biomech. Eng.*, vol. 136, no. 2, p. 021033, Feb. 2014.

[37] E. M. Arnold, S. R. Ward, R. L. Lieber, and S. L. Delp, "A model of the lower limb for analysis of human movement," *Ann. Biomed. Eng.*, vol. 38, no. 2, pp. 269–279, Feb. 2010.

[38] S. L. Delp and J. P. Loan, "A computational framework for simulating and analyzing human and animal movement," *Comput. Sci. Eng.*, vol. 2, no. 5, pp. 46–55, 2000.

[39] C. R. Smith, M. F. Vignos, R. L. Lenhart, J. Kaiser, and D. G. Thelen, "The influence of component alignment and ligament properties on tibiofemoral contact forces in total knee replacement," *J. Biomech. Eng.*, vol. 138, no. 2, pp. 21010–21017, Jan. 2016.

[40] C. Pizzolato *et al.*, "CEINMS: A toolbox to investigate the influence of different neural control solutions on the prediction of muscle excitation and joint moments during dynamic motor tasks," *J. Biomech.*, vol. 48, no. 14, pp. 3929–3936, Nov. 2015.

[41] M. Sartori, M. Reggiani, D. Farina, and D. G. Lloyd, "EMG-driven forward-dynamic estimation of muscle force and joint moment about multiple degrees of freedom in the human lower extremity," *PLoS ONE*, vol. 7, no. 12, p. e52618, Dec. 2012.

[42] P. Julkunen, P. Kiviranta, W. Wilson, J. S. Jurvelin, and R. K. Korhonen, "Characterization of articular cartilage by combining microscopic analysis with a fibril-reinforced finite-element model," *J. Biomech.*, vol. 40, no. 8, pp. 1862–1870, Jan. 2007.

[43] W. Wilson, "A comparison between mechano-electrochemical and biphasic swelling theories for soft hydrated tissues," *J. Biomech. Eng.*, vol. 127, no. 1, p. 158, Mar. 2005.

[44] W. Wilson, C. C. van Donkelaar, B. van Rietbergen, K. Ito, and R. Huiskes, "Erratum to 'Stresses in the local collagen network of articular cartilage: A poroviscoelastic fibril-reinforced finite element study' [Journal of Biomechanics 37 (2004) 357-366] and 'A fibril-reinforced poroviscoelastic swelling model for articular cartil," *J. Biomech.*, vol. 38, no. 10, pp. 2138–2140, Oct. 2005.

[45] P. Böttcher, M. Zeissler, J. Maierl, V. Grevel, and G. Oechtering, "Mapping of split-line pattern and cartilage thickness of selected donor and recipient sites for autologous osteochondral transplantation in the canine stifle joint," *Vet. Surg.*, vol. 38, no. 6, pp. 696–704, Aug. 2009.

[46] D. W. Goodwin, Y. Z. Wadghiri, H. Zhu, C. J. Vinton, E. D. Smith, and J. F. Dunn, "Macroscopic structure of articular cartilage of the tibial plateau: Influence of a characteristic matrix architecture on MRI appearance," *Amer. J. Roentgenol.*, vol. 182, no. 2, pp. 311–318, Feb. 2004.

[47] S. Below, S. P. Arnoczky, J. Dodds, C. Kooima, and N. Walter, "The split-line pattern of the distal femur: A consideration in the orientation of autologous cartilage grafts," *Arthroscopy J. Arthroscopic Related Surg.*, vol. 18, no. 6, pp. 613–617, Jul. 2002.

[48] A. Benninghoff, "Form und bau der gelenkknorpel in ihren beziehungen zur funktion," *Zeitschrift für Zellforsch*, vol. 2, no. 5, pp. 783–862, 1925.

[49] E. A. Makris, P. Hadidi, and K. A. Athanasiou, "The knee meniscus: Structure-function, pathophysiology, current repair techniques, and prospects for regeneration," *Biomaterials*, vol. 32, no. 30, pp. 7411–7431, 2011.

[50] D. F. Villegas, J. A. Maes, S. D. Magee, and T. L. H. Donahue, "Failure properties and strain distribution analysis of meniscal attachments," *J. Biomech.*, vol. 40, no. 12, pp. 2655–2662, 2007.

[51] L. Blankevoort and R. Huiskes, "Ligament-bone interaction in a three-dimensional model of the knee," *J. Biomech. Eng.*, vol. 113, no. 3, pp. 263–269, Aug. 1991.

[52] R. J. van Arkel, L. Modenese, A. T. M. Phillips, and J. R. T. Jeffers, "Hip abduction can prevent posterior edge loading of hip replacements," *J. Orthopaedic Res.*, vol. 31, no. 8, pp. 1172–1179, Aug. 2013.

[53] S. Gilbert *et al.*, "Dynamic contact mechanics on the tibial plateau of the human knee during activities of daily living," *J. Biomech.*, vol. 47, no. 9, pp. 2006–2012, 2014.

[54] D. L. Benoit, D. K. Ramsey, M. Lamontagne, L. Xu, P. Wretenberg, and P. Renström, "Effect of skin movement artifact on knee kinematics during gait and cutting motions measured *in vivo*," *Gait Posture*, vol. 24, no. 2, pp. 64–152, Oct. 2006.

[55] M. Kozanek *et al.*, "Tibiofemoral kinematics and condylar motion during the stance phase of gait," *J. Biomech.*, vol. 42, no. 12, pp. 1877–1884, Aug. 2009.

[56] V. Kefala *et al.*, "Assessment of knee kinematics in older adults using high-speed stereo radiography," *Med. Sci. Sports Exerc.*, vol. 49, no. 11, pp. 2260–2267, Nov. 2017.

[57] H. Marouane, A. Shirazi-Adl, and M. Adouni, "Alterations in knee contact forces and centers in stance phase of gait: A detailed lower extremity musculoskeletal model," *J. Biomech.*, vol. 49, no. 2, pp. 185–192, Jan. 2016.

[58] Z. F. Lerner, M. S. DeMers, S. L. Delp, and R. C. Browning, "How tibiofemoral alignment and contact locations affect predictions of medial and lateral tibiofemoral contact forces," *J. Biomech.*, vol. 48, no. 4, pp. 644–650, Feb. 2015.

[59] K. Manal and T. S. Buchanan, "An electromyogram-driven musculoskeletal model of the knee to predict *in vivo* joint contact forces during normal and novel gait patterns," *J. Biomech. Eng.*, vol. 135, no. 2, p. 021014, Feb. 2013.

[60] D. J. Saxby *et al.*, "Tibiofemoral contact forces during walking, running and sidestepping," *Gait Posture*, vol. 49, pp. 78–85, Sep. 2016.

[61] D. J. Saxby *et al.*, "Tibiofemoral contact forces in the anterior cruciate ligament-reconstructed knee," *Med. Sci. Sports Exerc.*, vol. 48, no. 11, pp. 2195–2206, Nov. 2016.

[62] G. K. Lenton *et al.*, "Tibiofemoral joint contact forces increase with load magnitude and walking speed but remain almost unchanged with different types of carried load," *PLoS ONE*, vol. 13, no. 11, Nov. 2018, Art. no. e0206859.

[63] C. R. Winby, D. G. Lloyd, T. F. Besier, and T. B. Kirk, "Muscle and external load contribution to knee joint contact loads during normal gait," *J. Biomech.*, vol. 42, no. 14, pp. 2294–2300, Oct. 2009.

[64] M. E. Mononen *et al.*, "A novel method to simulate the progression of collagen degeneration of cartilage in the knee: Data from the osteoarthritis initiative," *Sci. Rep.*, vol. 6, no. 1, p. 21415, Aug. 2016.

[65] F. Liu *et al.*, "*In vivo* tibiofemoral cartilage deformation during the stance phase of gait," *J. Biomech.*, vol. 43, no. 4, pp. 658–665, Mar. 2010.

[66] M. K. Liukkonen *et al.*, "Evaluation of the effect of bariatric surgery-induced weight loss on knee gait and cartilage degeneration," *J. Biomech. Eng.*, vol. 140, no. 4, pp. 041008-1–041008-11, Apr. 2018.

[67] M. Sartori, D. Farina, and D. G. Lloyd, "Hybrid neuromusculoskeletal modeling to best track joint moments using a balance between muscle excitations derived from electromyograms and optimization," *J. Biomech.*, vol. 47, no. 15, pp. 3613–3621, Nov. 2014.

[68] Z. I. Nejad *et al.*, "The capacity of generic musculoskeletal simulations to predict knee joint loading using the CAMS-knee datasets," *Ann. Biomed. Eng.*, vol. 48, no. 4, pp. 1430–1440, Jan. 2020.

[69] L. P. Räsänen, "Three dimensional patient-specific collagen architecture modulates cartilage responses in the knee joint during gait," *Comput. Methods Biomech. Biomed. Eng.*, vol. 19, no. 11, pp. 1225–1240, Aug. 2016.

[70] D. G. Lloyd and T. S. Buchanan, "Strategies of muscular support of varus and valgus isometric loads at the human knee," *J. Biomech.*, vol. 34, no. 10, pp. 1257–1267, Oct. 2001.

[71] L. Q. Zhang, D. Xu, G. Wang, and R. W. Hendrix, "Muscle strength in knee varus and valgus," *Med. Sci. Sports Exerc.*, vol. 33, no. 7, pp. 1194–1199, 2001.

[72] D. J. Saxby *et al.*, "Machine learning methods to support personalized neuromusculoskeletal modelling," *Biomech. Model. Mechanobiol.*, vol. 19, no. 4, pp. 1169–1185, Aug. 2020.